Catalysis Science & Technology

ROYAL SOCIETY OF CHEMISTRY

PAPER

View Article Online
View Journal | View Issue

Cite this: *Catal. Sci. Technol.*, 2023, **13**, 7181

On the mechanism of benzimidazole synthesis *via* copper-catalysed intramolecular *N*-arylation†

Xiaodong Jin, ‡ Yongjie Lin and Robert P. Davies *

Received 2nd June 2023,
Accepted 3rd November 2023

DOI: 10.1039/d3cy00767g

rsc.li/catalysis

Copper(I)-catalysed intramolecular Ullmann *N*-arylation has been widely used to synthesise benzimidazoles. However, the possible intermediates on the catalytic pathway and the role of the ancillary ligands in these systems have been seldom studied and are currently not fully understood, especially when compared to comparable intermolecular Ullmann reactions. Accordingly, this work explores the copper(I)-intramolecular *N*-arylation of 1,2-dimethylbenzimidazole, reporting on the solid-state structures of several copper(I) species with the reaction substrate and product. In addition, kinetic profiling using bis(tetra-*n*-butylphosphonium) malonate as a soluble base has been carried out, notably revealing negligible catalyst deactivation but significant catalyst inhibition. Based on these results an improved catalytic protocol using sub-mol% catalyst loading has been developed.

Introduction

Benzimidazoles are an important class of heterocycles comprising of benzene-fused imidazole scaffolds. They are often biologically active and therefore play an important role in pharmaceutical research.[1–3] Benzimidazoles are one of the most commonly encountered nitrogen heterocycles in U.S. FDA approved drugs, and their derivatives have shown activity for a wide range of applications including antiulcers, anthelmintics, antivirals, anticancer drugs, antimicrobials, analgesics and anti-inflammatory agents.[4]

The synthesis of benzimidazoles has therefore attracted great interest over the years.[5,6] The two most common strategies reported for the preparation of substituted benzimidazoles are condensation and intramolecular C–N cross coupling (Scheme 1). The condensation method forms two new C–N bonds by reacting 1,2-diaminoarenes with carboxylic acids[7–9] or aldehydes/oxidants.[10–12] However, this long-standing protocol has some drawbacks, including the use of strong acids and high reaction temperatures. The alternative newer intramolecular cross-coupling method employs amidines as starting materials and can operate under milder conditions. The key ring-forming step is a metal-catalysed intramolecular C–N cross coupling using *N*′-(2-halogenphenyl)-*N*-substituted-ethanimidamide. Many different combinations of pre-catalyst and auxiliary ligand have been employed for these intramolecular cyclizations, including Pd-phosphine catalysts,[13] Cu_2O or CuI,[14,15] CuO nanoparticles,[16] and even transition-metal-free conditions (for example, KOH mediated couplings in DMSO at 120 °C).[17]

Recent advances in intermolecular copper-catalysed *N*-arylation (including the introduction of ancillary ligands) have led to higher yields, improved reliability, lower catalyst loadings, and milder reaction conditions.[18,19] In addition, it has permitted the use of more challenging substrates such as aryl chlorides. Over recent years, studies on the mechanism of the intermolecular *N*-arylation (Ullmann amination) reaction by our group and others has led to a much improved understanding of these systems.[20–26] However, to date, mechanistic studies on related intramolecular Ullmann reactions are rare, and advances in the understanding and methodology for intermolecular coupling has yet to be fully transitioned to these intramolecular systems.

Therefore, in order to build an improved mechanistic understanding of copper-catalysed intramolecular *N*-arylation

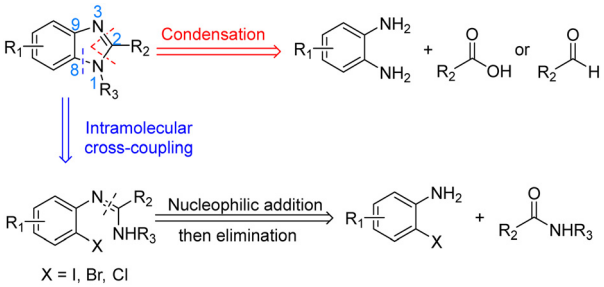

Scheme 1 Retrosynthetic synthesis of benzimidazoles.

Department of Chemistry, Molecular Sciences Research Hub, Imperial College White City Campus, Wood Lane, London W12 0BZ, UK.
E-mail: r.davies@imperial.ac.uk

† Electronic supplementary information (ESI) available: Additional experimental and crystallographic details. CCDC 2263362 to 2263367. For ESI and crystallographic data in CIF or other electronic format see DOI: https://doi.org/10.1039/d3cy00767g

‡ Current address: Department of Chemistry, Xi'an Jiaotong-Liverpool University, Suzhou 215123, China.

and to identify any differences with the intermolecular systems, a series of reactivity and mechanism studies have been carried out in this work for the synthetically important preparation of benzimidazoles. The solid-state structures of several copper(I) species derived from the reaction starting materials have been obtained. These structures reveal a range of potential coordination modes adopted by the substrate and auxiliary ligand (where present) with the copper(I) centre. The incorporation of both the aryl halide and amine functionalities within the same substrate permits additional insight not often accessible using intermolecular systems.

Detailed kinetic profiling using reaction progress kinetic analysis (RPKA) methodology[27,28] has also been carried out to study the potential catalyst inhibition and deactivation pathways which may occur during the catalytic process, and to determine the rate dependence on the concentration of reactants. Based on these studies, an improved protocol capable of operating at sub-mol% copper catalyst loadings has been developed.

Results and discussion

TBPM promoted copper(I)-catalysed intramolecular *N*-arylation

The copper(I)-catalysed synthesis of 1,2-dimethylbenzimidazole (**2**) *via* intramolecular C–N cross-coupling of *N*′-(2-halogenphenyl)-*N*-methylethanimidamide (**1a–1c**) was selected as a model reaction for these studies. The soluble ionic base *n*-tetrabutylphosphonium malonate (TBPM) has previously been reported in the literature to promote copper-catalysed inter-molecular *N*-arylation reactions,[23,25,29] and was employed here as the base. Significantly, the excellent solubility of TBPM in the reaction mixture precludes any base mass transfer effects. In terms of substrate reactivity, aryl iodide (**1a**) was observed to be the most reactive with self-cyclisation occurring at room temperature (38% yield) even without a catalyst, and over 99% yield of the cyclised product was obtained with the addition of 5 mol% CuI (Table 1, entries 1 and 2). The aryl bromide **1b** also gave near quantitative conversions in the presence of the catalyst, though no background reaction without a catalyst was observed in this case (entries 3 and 4). The less reactive aryl chloride **1c** required both the copper catalyst and high reaction temperatures (130 °C) to give satisfactory yields (entries 5 and 6).

Table 1 TBPM promoted copper(I)-catalysed intramolecular *N*-arylation

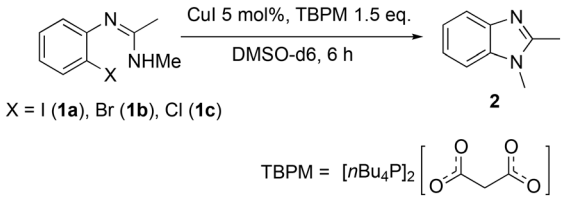

Entry	Substrate	X =	CuI	Temp. (°C)	Yield (%)
1	**1a**	I	—	r.t.	38
2	**1a**	I	5%	r.t.	>99
3	**1b**	Br	—	r.t.	0
4	**1b**	Br	5%	r.t.	>99
5	**1c**	Cl	—	130	0
6	**1c**	Cl	5%	130	80

Reaction yield was measured by ^{1}H NMR using naphthalene as internal standard.

Copper(I) complexes: isolation and characterisation

In order to investigate the different complexes that might be present in the reaction mixture, a study of the solid-state structures of potential copper containing intermediates was carried out. Single crystals were obtained by reacting aryl halides (**1a–1d**) with mesitylcopper(I) followed by the recrystallisation of the resultant copper(I) complexes from toluene/hexane (Scheme 2).

For the more reactive aryl iodide (**1a**) and bromide (**1b**), intramolecular amination occurred readily giving complexes in which the imine group of the cyclised benzimidazole product **2** coordinates to a copper(I) centre. However, the less reactive aryl chloride (**1c**) and fluoride (**1d**) remained uncyclized with the negative charge on the substrate delocalised over the imidazole N–C–N unit.

Reaction of aryl iodide **1a** with mesitylcopper led to the formation of crystals which were identified, using single crystal X-ray diffraction, as the tetramer Cu_4I_4**2**$_4$ (Fig. 1a). Each copper(I) centre forms bonds with either two or three bridging iodide anions and one nitrogen (imine) atom. Cu–N distances are 1.957(3) and 1.980(3) Å. This gives rise to a four rung CuI twisted ladder structure in which the copper atoms adopt a close to planar rhombic Cu_4 arrangement. Closer inspection of the benzimidazole groups within the copper complex reveals them to stack in an almost head-to-tail confirmation (offset 156°). Adjacent imidazole rings stack directly on one another with a distance between the centroids of 3.536 and 3.614 Å. A search of the literature shows benzimidazole-ligated copper(I) iodide complexes to have been reported with monomeric, dimeric, tetrameric, and polymeric CuI units. However, only a small number of tetrameric clusters are known, all of which contain cubic Cu_4I_4 units based around a tetrahedral arrangement of copper atoms (Fig. 1b).[30–32] The unique twisted ladder cluster in Cu_4I_4**2**$_4$ maybe due to the stabilisation obtained from the π-stacking combined with the steric requirements of the methyl group on the carbon of the imidazole ring.

Similar to **1a**, intramolecular amination also occurred when aryl bromide **1b** was reacted with mesitylcopper(I). However, in this case, a different aggregation state was

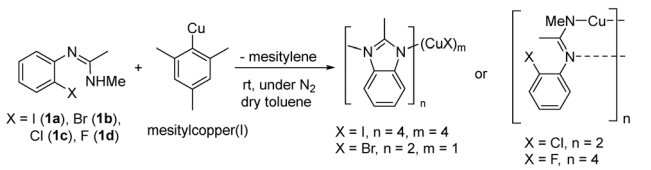

Scheme 2 Synthesis of new copper(I) complexes in this work.

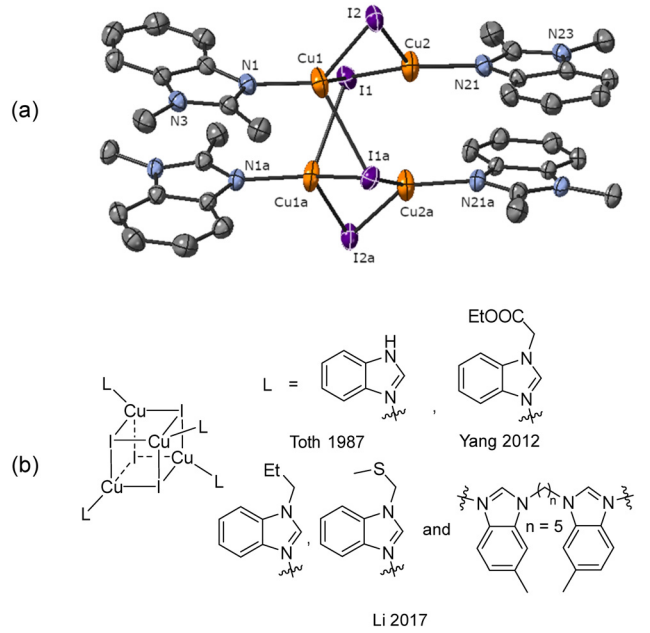

Fig. 1 (a) Solid-state structure of Cu_4I_4**2**$_4$; thermal ellipsoids are set at 50% probability and hydrogen atoms are omitted for clarity. (b) Benzimidazole ligated Cu_4I_4 complexes reported in the literature.[30–32]

observed in the solid state with just one CuBr unit coordinating to two molecules of **2** (Fig. 2a). The CuBr**2**$_2$ complex has comparable Cu–N bond distances (1.9718(18) and 1.9853(18) Å) to those in the Cu_4I_4**2**$_4$ tetramer. Two other examples of benzimidazole ligated copper(I) bromide complexes have previously been reported in the literature (Fig. 2b).[33,34]

Due to the stronger aryl-halide bond in **1c**, intramolecular amination did not proceed in the reaction of mesitylcopper(I) with **1c** at room temperature. X-ray diffraction studies instead revealed the formation of the dimeric structure Cu_2**1c**′$_2$ (where **1c**′ is deprotonated **1c**) comprising of a nearly planar

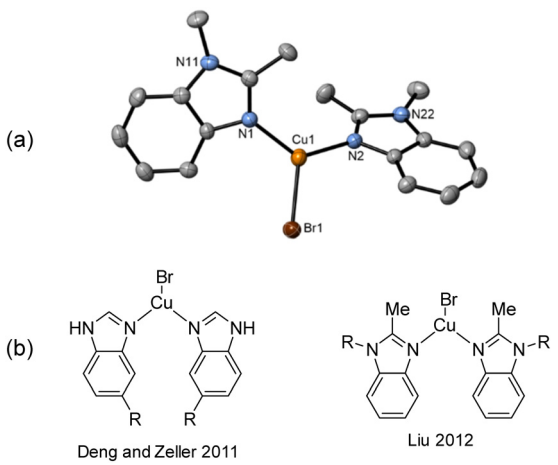

Fig. 2 (a) Solid-state structure of CuBr**2**$_2$; thermal ellipsoids are set at 50% probability and hydrogen atoms are omitted for clarity. (b) Benzimidazole ligated CuBr complexes reported in literature.[33,34]

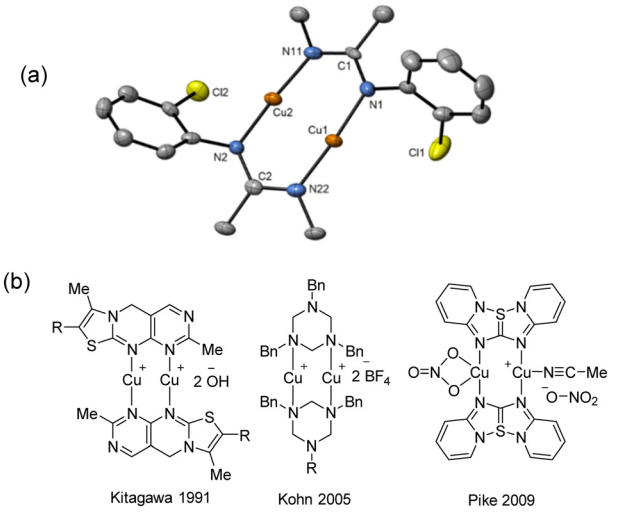

Fig. 3 (a) Solid-state structure of one of the two independent molecules in Cu_2**1c**′$_2$; thermal ellipsoids are set at 50% probability and hydrogen atoms are omitted for clarity. (b) Copper(I) complexes containing planar $Cu_2N_4C_2$ 8-membered rings.[35–37]

$Cu_2N_4C_2$ 8-membered ring (Cu···Cu distance 2.441 Å). The secondary amine group in **1c** has been deprotonated by mesitylcopper(I) to give a Cu–N bond. The Cu–N bonds in Cu_2**1c**′$_2$ are shorter (mean 1.882°) than those in either Cu_4I_4**2**$_4$ or CuBr**2**$_2$. Furthermore, the C1–N1 and C1–N11 bond distances (1.344(6) and 1.314(6) Å) are indicative of at least partial delocalization of the negative charge over the amidinate units. Although several copper(I) complexes containing planar $Cu_2N_4C_2$ 8-membered rings have been reported in the literature,[35–37] these differ from Cu_2**1c**′$_2$ by virtue of being cationic, with the copper centers ligated by neutral bridging ligands (Fig. 3b).

When aryl fluoride **1d** was employed in the reaction with mesitylcopper(I), a copper complex with a tetrameric aggregation state was observed (Fig. 4a). Cu_4**1d**′$_4$ (where **1d**′ is deprotonated **1d**) contains a folded $Cu_4N_4C_4$ 16-membered ring with a central distorted rhombic Cu_4 core (Fig. 4b). Similar to Cu_2**1c**′$_2$, the negative charge is delocalized within the N–C–N units with, for example, C1–N1 and C1–N11 bond distances of 1.343(5) Å and 1.313(5) Å respectively. Similar copper(I) complexes containing 16-membered $Cu_4N_8C_4$ (ref. 38) or Cu_4N_{12} (ref. 39–43) rings, planar Cu_4 arrangements, and close to linear N–Cu–N coordination have been reported in the literature (Fig. 4c).

Given that the addition of 1,10-phenanthroline (**L1**) has been shown to increase product yield in copper catalysed benzoxazole synthesis,[44] the interaction of **L1** with Cu_4**1d**′$_4$ was also investigated. Thus, reaction of **1d** with mesitylcopper(I) in the presence of **L1** gave crystals which were characterized by X-ray diffraction as Cu_2(**1d**′)$_2$(**L1**) (Fig. 5). The addition of **L1** therefore leads to a dimeric complex containing an 8-membered $Cu_2N_4C_2$ ring. This contrasts to the tetramer Cu_4**1d**′$_4$ observed without the presence of **L1** (Fig. 4a). The structure of Cu_2(**1d**′)$_2$(**L1**) also

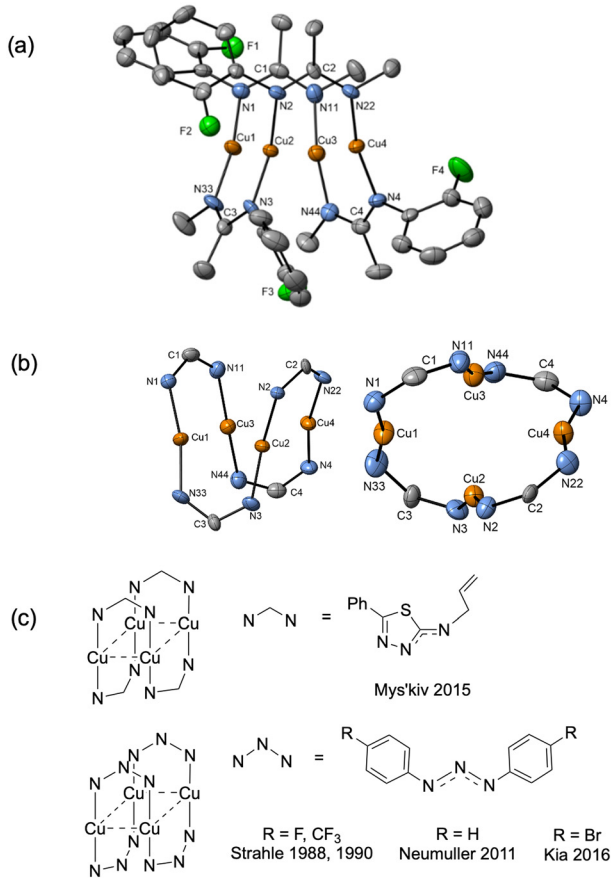

Fig. 4 (a) Solid-state structures of Cu_4**1d′**$_4$; thermal ellipsoids are set at 50% probability and hydrogen atoms are omitted for clarity. (b) Different views of the $Cu_4N_4C_4$ 16-membered ring. (c) Copper(I) complexes containing a 16-membered ring and N–Cu–N coordination.[38–43]

differs from the dimeric structure of Cu_2**1c′**$_2$ (Fig. 3a) as the two aryl halides adopt a head-to-head arrangement in Cu_2(**1d′**)$_2$(**L1**), rather than the head-to-tail arrangement in Cu_2**1c′**$_2$. The presence of **L1** leads to a significant elongation of the Cu1–N1 bond (1.999(2) Å) when compared to the Cu2–N3 bond (1.859(2) Å). This can be attributed to the increased coordination number (four) of Cu1 compared to Cu2 (which is two coordinate). The delocalization of the negative charge within the N–C–N unit was also confirmed by the C–N bond distances (N1–C2 = 1.307(4) Å; C2–N3 = 1.352(4) Å).

To confirm whether these copper(I) complexes are feasible reaction intermediates, the reactivity of Cu_2**1c′**$_2$ was studied by heating the complex, with or without **L1**, to 110 °C in DMSO (Table 2). Cu_2**1c′**$_2$ reacts at this higher temperature to give the desired cyclized benzimidazole product **2**, supporting its viability as an intermediate on the reaction pathway. Furthermore, addition of **L1** gave an improved yield for this reaction (see Fig. 11 and discussion later for a comparison of catalytic reaction rates with different ligands).

Overall, the solid-state structures of these copper(I) complexes furnish some novel insights into copper coordination modes and aggregation states with amidinate and imidazole substrates. In all the uncyclized products, it is interesting to note that the copper centers coordinate to the amidinate nitrogens and thus remain relatively distant from the aryl-halide bonds. If a similar motif were adopted under the catalytic reaction conditions it is likely that aryl-halide activation would require the involvement of an additional copper center for the intramolecular cyclization reaction to proceed. However, it is difficult to draw any direct parallels between the solid-state structures and catalyst speciation in the reaction due to the different conditions employed (solvent, presence of base, temperature *etc.*). Therefore, an alternative approach was also employed based on kinetic measurements of the actual catalytic system as detailed below.

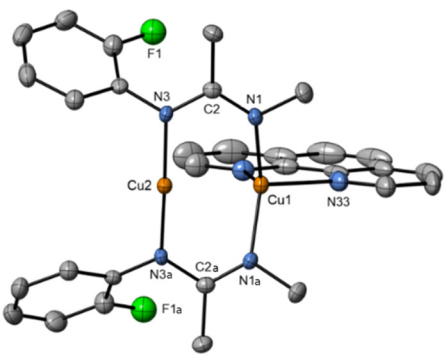

Fig. 5 Solid-state structure of Cu_2(**3d′**)$_2$(**L2**). Thermal ellipsoids are set at 50% probability and hydrogen atoms are omitted for clarity.

Reaction kinetic studies

In order determine the rate dependence in reactants as well as build a better understanding of the catalyst performance, the intramolecular *N*-arylation reaction was profiled using a superCRC calorimeter (see the ESI† for full details). Initial reaction calorimetry studies focused upon the rate dependence on catalyst concentration, with the order in the catalyst determined by comparing the graphical rate equations obtained using different catalyst concentrations.[27]

Table 2 Reactivity of Cu_2**1c′**$_2$ toward benzimidazole synthesis

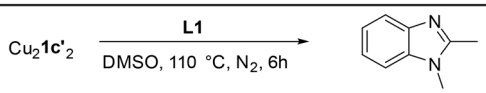

Entry	Substrate	**L1**	**2** (%)
1	Cu_2**1c′**$_2$	—	65
2	Cu_2**1c′**$_2$	1 equiv.	89

The reaction was carried out by heating the copper(I) complex (0.1 mmol) in DMSO (1 mL) with or without **L1** (0.1 mmol). The yield of **2** was determined by ^{1}H NMR using naphthalene as internal standard.

A positive non-integer order in $[Cu]_{total}$ was observed (Fig. 6a) with 'best fit' reaction rate plots obtained by normalising by $[Cu]_{total}^{1.35}$ (Fig. 6b). Non-integer orders in catalyst concentration have been used to infer catalyst deactivation or off-cycle equilibrium(s), whereas an order in [catalyst] greater than one can indicate catalyst inhibition or more than one catalytic species being involved in the rate determining step.[45] This later scenario could fit with observations from the solid-state studies where the copper centre in the metalated aryl halide would seem to be sited too distant from the aryl-halide bond to permit oxidative addition at this centre, and hence an additional catalytic copper centre would be required for the rate limiting oxidative addition step. The following experiments explore this possibility in more detail. It is noteworthy that this behaviour therefore differs to that observed for intermolecular Ullmann aminations where generally first order reactions in [Cu] have been reported and where amide coordination/deprotonation and aryl halide activation occurs at the same copper centre.[22,24,25]

A "same excess" experiment was carried out to investigate potential catalyst deactivation and/or inhibition. This experiment involved reducing $[TBPM]_0$ and $[\mathbf{1b}]_0$ in 0.0250 M increments, whilst keeping the excess [*e*] constant at 0.0500 (Fig. 7a). The marked lack of overlay of the graphical rate equations indicates that strong catalyst deactivation and/or inhibition processes are occurring. To distinguish between deactivation and inhibition, a "same excess" experiment was carried out with the addition of the three reaction products, namely 1,2-dimethylbenzimidazole (**2**), the mono-anion of malonic acid (MalH) and tetra-(*n*-butyl)phosphonium bromide (TBPB) (Fig. 7b) – note that in these experiments all reagents and additives are fully dissolved to give a homogeneous solution. All three graphical rate equations now overlayed one another very well, indicating that catalyst

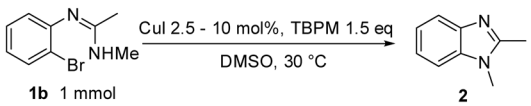

Symbol	$[CuI]_0$ (M)	$[\mathbf{1b}]_0$ (M)	$[TBPM]_0$ (M)	[*e*] (M)
●	0.0100	0.1000	0.1500	0.0500
●	0.0050	0.1000	0.1500	0.0500
●	0.0025	0.1000	0.1500	0.0500

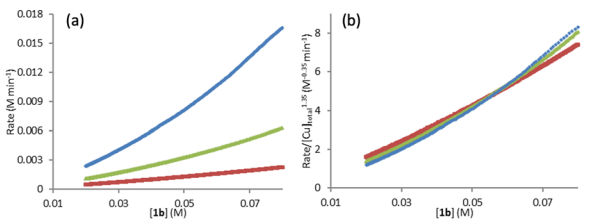

Fig. 6 Rate dependence on [CuI]: (a) comparison of graphical rate equations using different [CuI]; (b) the reaction rate is normalized by $[Cu]^{1.35}$ to show the best fit overlap.

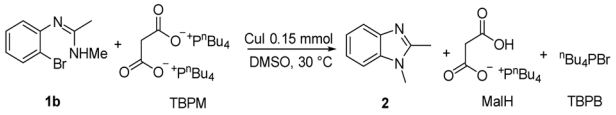

Symbol	$[\mathbf{1b}]_0$ (M)	$[TBPM]_0$ (M)	[*e*] (M)	$[\mathbf{2}]_0$ (M)	$[MalH]_0$ (M)	$[TBPB]_0$ (M)
(a) ●	0.1000	0.1500	0.0500	0	0	0
(a) ●	0.0750	0.1250	0.0500	0	0	0
(a) ●	0.0500	0.1000	0.0500	0	0	0
(b) ●	0.1000	0.1500	0.0500	0	0	0
(b) ●	0.0750	0.1250	0.0500	0.0250	0.0250	0.2500
(b) ●	0.0500	0.1000	0.0500	0.0500	0.0500	0.0500

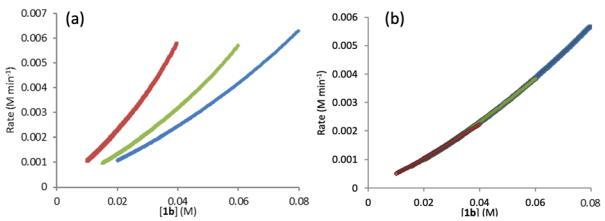

Fig. 7 (a) "Same excess" experiment: graphical rate against [**1b**]; (b) "same excess" experiment with addition of corresponding amounts of **2**, MalH and TBPB.

inhibition is occurring and any catalyst deactivation is negligible. This differs from our previous calorimetry study on intermolecular copper-catalysed *N*-arylation in which catalyst deactivation occurred and catalyst inhibition was negligible.[36]

As the initial inhibition experiment used addition of all products together ([**2**], [MalH] and [TBPB]), the inhibition cause by each component was also studied individually, starting with benzimidazole **2** (Fig. 8). This revealed a significant negative order in [**2**] which could be due to an off-cycle process involving coordination of **2** to the copper center. The predilection of **2** to coordinate to Cu(I) has already been observed in the solid-state studies (Fig. 1 and 2) and can be explained by the accessible exocyclic lone pair on the imidazole nitrogen which readily coordinates to the copper center. Inhibition experiments using the mono-anion of malonic acid (MalH) and tetra-(*n*-butyl)phosphonium bromide (TBPB) both showed less pronounced negative influences on the reaction rate (see the ESI† for plots), which can be rationalized respectively by the formation of an inactive diligated copper(I) complex with MalH and variations in solution conductivity with TBPB.

Different excess experiments[28] were then carried out to determine the rate dependences on [**1b**] and [TBPM]. Fig. 9 shows the graphical equations for [**1b**]. The reaction rate can be normalized by $[\mathbf{1b}]^1$ indicating that the reaction is first order in the aryl bromide starting material (Fig. 9b).

The rate dependence on [TBPM] was found to be approximately negative first order (Fig. 10). This shows that

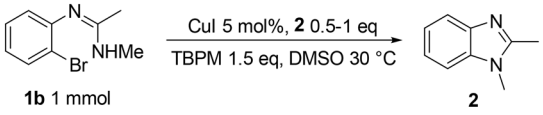

Symbol	[1b]$_0$ (M)	[TBPM]$_0$ (M)	[*e*] (M)	[2]$_0$ (M)
●	0.1000	0.1500	0.0500	0
●	0.1000	0.1500	0.0500	0.0500
●	0.1000	0.1500	0.0500	0.1000

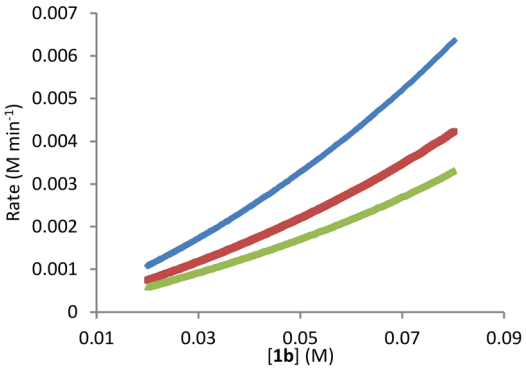

Fig. 8 Catalyst inhibition experiment: graphical rate against [**1b**] with addition of 1,2-dimethylbenzimidazole **2**.

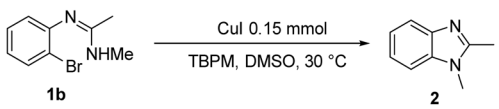

Symbol	[1b]$_0$ (M)	[TBPM]$_0$ (M)	[*e*] (M)
●	0.1000	0.1500	0.0500
●	0.0750	0.1500	0.0750
●	0.0500	0.1500	0.1000

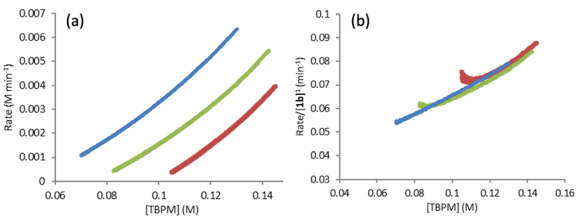

Fig. 9 "Different excess" experiment: (a) graphical rate equation against [TBPM]; (b) normalised reaction rate by [**1b**]^1 and overlapped.

higher TBPM loading can inhibit the reaction to give a slower overall rate. A negative rate dependence on [TBPM] was also reported in TBPM promoted Cu(I)-catalysed inter-molecular *N*-arylation where this was rationalised by the formation of an inactive (off-cycle) di(malonate) copper(I) complex.[25]

Based upon these kinetic studies and existing literature knowledge on related systems,[23] we now put forward a postulated reaction mechanism (Scheme 3). The presence of two catalytic species in the rate limiting step, product inhibition, and a negative order in TBPM make this a

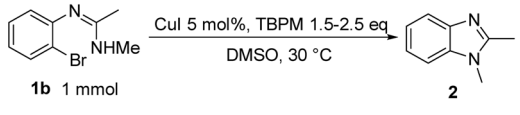

Symbol	[1b]$_0$ (M)	[TBPM]$_0$ (M)	[*e*] (M)
●	0.1000	0.1500	0.0500
●	0.1000	0.2000	0.1000
●	0.1000	0.2500	0.1500

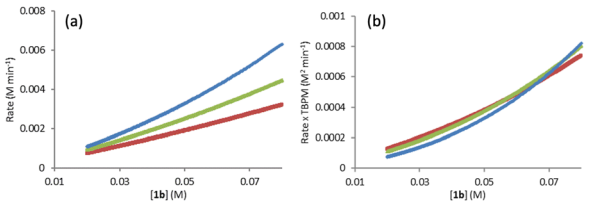

Fig. 10 (a) "Different excess experiment": graphical rate against [**1b**]; (b) normalized rate by [TBPM]$^{-1}$.

challenging system to study, however some key salient similarities and differences can be observed between this intramolecular coupling and more widely studied intermolecular couplings.

Rate dependence on [ArBr] (1st order) and [TBPM] (approximately negative 1st order) are in agreement with the literature for intermolecular Ullmann reactions.[23] Also the proposed oxidative addition rate limiting step which takes place at a copper center with a malonate XX-type ligand is the same. However a catalyst order greater than 1 is suggestive of two catalytic species reacting on a cycle and a 'parent-offspring species mechanism'[45] seems most

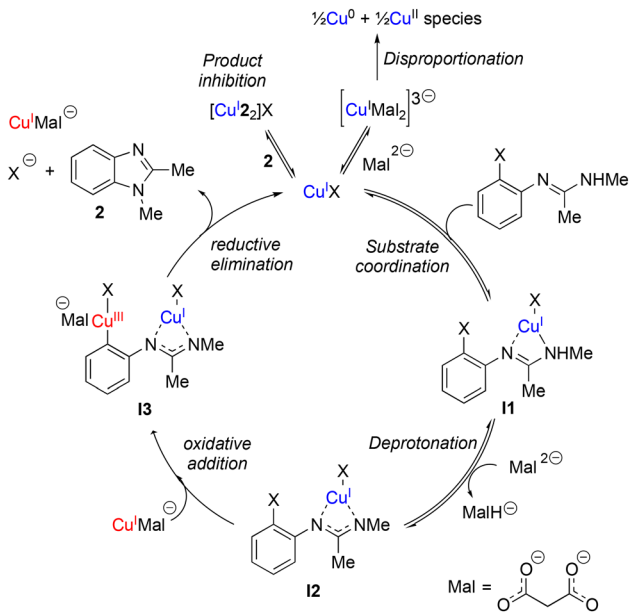

Scheme 3 Proposed mechanism for TBPM promoted copper(I)-catalysed intramolecular *N*-arylation.

probable. One copper centre aids with the deprotonation of the amidine unit (required due to the relative weakness of the TBPM base[23]) whilst the other copper centre facilitates the aryl halide oxidative addition step. Although all catalytic on-cycle species are shown in Scheme 3 as monomeric, aggregates similar to those observed in the X-ray diffraction studies cannot be ruled out.

Catalyst inhibition by the imidazole product (**2**) plays a significant role as the reaction progresses towards completion as revealed by the kinetic studies as shown in Scheme 3 as an off-cycle equilibrium. Additional equilibrium due to excess Mal coordination are also inhibitory to a lesser extent but are not shown in Scheme 3 for clarity.

Reaction optimisation

The addition of an ancillary ligand has previously been shown to help improve yields and reactions rates for Ullmann arylations when organic bases such as TBPM are used.[24] However the use of organic bases with an ancillary ligand for intramolecular Ullmann arylations have not yet been investigated, hence TBPM promoted copper(I)-catalysed intramolecular *N*-arylation was also carried out in the presence of ancillary ligands. Unfortunately, none of the ligands studied (**L1**–**L4**) led to an improvement in the reaction rate compared to the ligandless system (Fig. 11). Moreover, increasing [**L1**] to 20 mol% resulted in an even lower reaction rate. Competition between the ancillary ligand and the malonate anion from TBPM for coordination to the metal center and the fact that malonate is already a good ligand for the reaction would explain these observations.

Given the absence of any catalyst decomposition processes (as shown by the "same excess" experiments described above), attempts were made to lower the copper(I) loading to

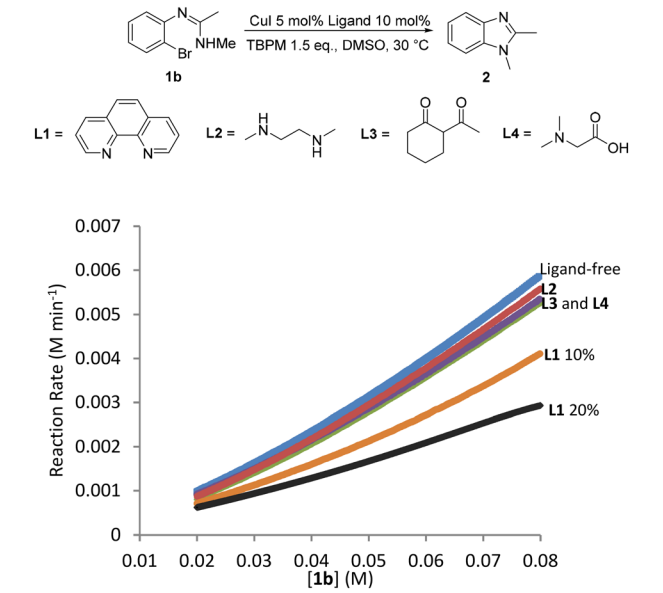

Fig. 11 *In situ* ligand screening by calorimetry.

Table 3 Sub-mol% copper(I)-catalyzed intramolecular *N*-arylation

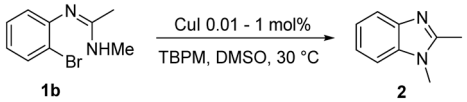

1b 2

Entry	CuI (mol%)	Temp. (°C)	Time (h)	Yield (%)
1	—	22	72	n.r.
2	0.1	22	72	91
3	1	22	72	>99
4	—	110	24	63
5	0.1	110	3	>99

sub-mol% levels (Table 3). Pleasingly, it was shown that the reaction can proceed with catalyst loadings as low as 0.1 mol% CuI and still give satisfactory yields even at room temperature (entry 2). Over 99% yield can be achieved within 3 hours by increasing the reaction temperature to 110 °C (entry 5), although it should be noted that at this higher temperate the reaction can also proceed without a catalyst, although longer reaction times are required and the yield is significantly lower (entry 4).

Conclusion

New insights into the reactivity and mechanism of copper-catalysed intramolecular *N*-arylation for the synthesis of benzimidazoles have been obtained, including the solid-state structures of copper(I) complexes with the amidinate substrate and benzimidazole product. For aryl iodide and aryl bromide substrates, cyclisation occurred readily when they were treated with mesitylcopper(I) to give 1,2-dimetylbenzimidazole ligated copper(I) complexes $Cu_4I_4\mathbf{2}_4$ and $CuBr\mathbf{2}_2$. The less reactive aryl chloride and fluoride substrates were found to form dimeric $(Cu_2\mathbf{1c}'_2)$ and tetrameric $(Cu_4\mathbf{1d}'_4)$ complexes respectively in which the aryl halide bond remained unreacted. Moreover, the solid-state structure of a 1,10-phenanthroline (**L1**) ligated intermediate $(Cu_2(\mathbf{1d}')_2(\mathbf{L1}))$ was reported revealing how **L1** can interact with just one of the metal centres.

Kinetic profiling of the intramolecular reaction was carried out using RPKA methods and *in situ* monitoring by a calorimeter. An organic ionic base (TBPM) was used in the reaction to avoid any base mass transfer effects and to allow comparison with similar intermolecular Ullmann couplings using this base.[23] Several parallels were observed between the intramolecular and intermolecular Ullmann couplings, notably the same rate dependence on [ArBr] (1st order) and [TBPM] (approximately negative 1st order). However, several significant differences were also found. Most notably, the rate dependence study on catalyst concentration reveals a complex order in $[Cu]_{total}$ ($1 < \text{order} < 2$), suggestive of two catalytic species reacting on a cycle in a parent-offspring species mechanism. The solid-state structures of $(Cu_2\mathbf{1c}'_2)$ and $(Cu_4\mathbf{1d}'_4)$ hint how one Cu centre might coordinate to the amidine functionality and aid its deprotonation, whilst the other facilitates activation

of the aryl halide moiety *via* oxidative addition. Same excess experiments reveal high levels of catalyst inhibition by the product **2** which can be attributed to strong interactions between the readily accessible exocyclic nitrogen lone pair on benzimidazole and the copper centres – a similar motif was also observed in the solid-state structures of $Cu_4I_4\mathbf{2}_4$ and $CuBr\mathbf{2}_2$. This highlights how small changes in the reaction components can have significant impact on the overall reaction kinetics. Based on these findings, we have been able to propose a new intramolecular sub-mol% copper(I)-catalysed process for the preparation of benzimidazoles. Further work is ongoing to further improve the scope of this reaction in terms of substrates and base.

Conflicts of interest

There are no conflicts of interest to declare.

Acknowledgements

The authors gratefully acknowledge Dr Andrew White for help with collecting and solving the crystal structure data.

Notes and references

1 B. Narasimhan, D. Sharma and P. Kumar, *Med. Chem. Res.*, 2010, **21**, 269–283.
2 K. Shah, S. Chhabra, S. K. Shrivastava and P. Mishra, *Med. Chem. Res.*, 2013, **22**, 5077–5104.
3 Y. Bansal and O. Silakari, *Bioorg. Med. Chem.*, 2012, **20**, 6208–6236.
4 R. Zou, K. R. Ayres, J. C. Drach and L. B. Townsend, *J. Med. Chem.*, 1996, **39**, 3477–3482.
5 M. Faheem, A. Rathaur, A. Pandey, V. Kumar Singh and A. K. Tiwari, *ChemistrySelect*, 2020, **5**, 3981–3994.
6 V. A. S. Pardeshi, N. S. Chundawat, S. I. Pathan, P. Sukhwal, T. P. S. Chundawat and G. P. Singh, *Synth. Commun.*, 2020, **51**, 485–513.
7 J. B. Wright, *Chem. Rev.*, 1951, **48**, 397–541.
8 S.-Y. Lin, Y. Isome, E. Stewart, J.-F. Liu, D. Yohannes and L. Yu, *Tetrahedron Lett.*, 2006, **47**, 2883–2886.
9 X. Wen, J. E. Bakali, R. Deprez-Poulain and B. Deprez, *Tetrahedron Lett.*, 2012, **53**, 2440–2443.
10 C. Mukhopadhyay and P. K. Tapaswi, *Tetrahedron Lett.*, 2008, **49**, 6237–6240.
11 M. Adharvana Chari, D. Shobha and T. Sasaki, *Tetrahedron Lett.*, 2011, **52**, 5575–5580.
12 S. M. Inamdar, V. K. More and S. K. Mandal, *Tetrahedron Lett.*, 2013, **54**, 579–583.
13 N. Zheng, K. W. Anderson, X. Huang, H. N. Nguyen and S. L. Buchwald, *Angew. Chem.*, 2007, **119**, 7653–7656.
14 J. Peng, M. Ye, C. Zong, F. Hu, L. Feng, X. Wang, Y. Wang and C. Chen, *J. Org. Chem.*, 2011, **76**, 716–719.
15 K. Liubchak, K. Nazarenko and A. Tolmachev, *Tetrahedron*, 2012, **68**, 2993–3000.
16 P. Saha, T. Ramana, N. Purkait, M. A. Ali, R. Paul and T. Punniyamurthy, *J. Org. Chem.*, 2009, **74**, 8719–8725.
17 H. Baars, A. Beyer, S. V. Kohlhepp and C. Bolm, *Org. Lett.*, 2014, **16**, 536–539.
18 S. Bhunia, G. G. Pawar, S. V. Kumar, Y. Jiang and D. Ma, *Angew. Chem., Int. Ed.*, 2017, **56**, 16136–16179.
19 G. Evano, N. Blanchard and M. Toumi, *Chem. Rev.*, 2008, **108**, 3054–3131.
20 E. Sperotto, G. P. van Klink, G. van Koten and J. G. de Vries, *Dalton Trans.*, 2010, **39**, 10338–10351.
21 C. Sambiagio, S. P. Marsden, A. J. Blacker and P. C. McGowan, *Chem. Soc. Rev.*, 2014, **43**, 3525–3550.
22 X. Ma and R. P. Davies, *Adv. Synth. Catal.*, 2022, **364**, 2023–2031.
23 Q. A. Lo, D. Sale, D. C. Braddock and R. P. Davies, *Eur. J. Org. Chem.*, 2019, **2019**, 1944–1951.
24 Q. A. Lo, D. Sale, D. C. Braddock and R. P. Davies, *ACS Catal.*, 2017, **8**, 101–109.
25 S. Sung, D. Sale, D. C. Braddock, A. Armstrong, C. Brennan and R. P. Davies, *ACS Catal.*, 2016, **6**, 3965–3974.
26 S. Sung, D. C. Braddock, A. Armstrong, C. Brennan, D. Sale, A. J. White and R. P. Davies, *Chemistry*, 2015, **21**, 7179–7192.
27 D. G. Blackmond, *J. Am. Chem. Soc.*, 2015, **137**, 10852–10866.
28 D. G. Blackmond, *Angew. Chem., Int. Ed.*, 2005, **44**, 4302–4320.
29 C. T. Yang, Y. Fu, Y. B. Huang, J. Yi, Q. X. Guo and L. Liu, *Angew. Chem., Int. Ed.*, 2009, **48**, 7398–7401.
30 Y. Fang, W. Liu, S. J. Teat, G. Dey, Z. Shen, L. An, D. Yu, L. Wang, D. M. O'Carroll and J. Li, *Adv. Funct. Mater.*, 2017, **27**, 1603444.
31 L. Yang and Z. Zhang, *Acta Crystallogr., Sect. E: Struct. Rep. Online*, 2012, **68**, m796.
32 A. Toth, C. Floriani, A. Chiesi-Villa and C. Guastini, *Inorg. Chem.*, 1987, **26**, 3897–3902.
33 X. Wang, C. B. Liu, Y. S. Yan, S. T. Wang and L. Liu, *Acta Crystallogr., Sect. E: Struct. Rep. Online*, 2012, **68**, m153.
34 L. Ma, Y.-C. Qiu, G. Peng, J.-B. Cai, H. Deng and M. Zeller, *CrystEngComm*, 2011, **13**, 3852.
35 S. Kitagawa, S. Matsuyama, M. Munakata, N. Osawa and H. Masuda, *J. Chem. Soc., Dalton Trans.*, 1991, 1717.
36 R. D. Kohn, Z. Pan, M. Haufe and G. Kociok-Kohn, *Dalton Trans.*, 2005, 2793–2797.
37 A. Saxena, E. C. Dugan, J. Liaw, M. D. Dembo and R. D. Pike, *Polyhedron*, 2009, **28**, 4017–4031.
38 Y. I. Slyvka, E. A. Goreshnik, B. R. Ardan, G. Veryasov, D. Morozov and M. G. Mys'kiv, *J. Mol. Struct.*, 2015, **1086**, 125–130.
39 E. Hartmann and J. Strähle, *Z. Naturforsch., B: J. Chem. Sci.*, 1988, **43**, 818–824.
40 E. Hartmann and J. Strähle, *Z. Anorg. Allg. Chem.*, 1990, **583**, 31–40.
41 M. Hörner, H. Fenner, W. Hiller and J. Beck, *Acta Crystallogr., Sect. C: Cryst. Struct. Commun.*, 1989, **45**, 204–206.
42 C. Lego and B. Neumüller, *Z. Anorg. Allg. Chem.*, 2011, **637**, 1784–1789.
43 R. Kia, *Inorg. Chim. Acta*, 2016, **446**, 32–40.

44 G. Altenhoff and F. Glorius, *Adv. Synth. Catal.*, 2004, **346**, 1661–1664.

45 C. Alamillo-Ferrer, G. Hutchinson and J. Burés, *Nat. Rev. Chem.*, 2022, **7**, 26–34.